



Article

Time-Domain Electromagnetic Noise Suppression Using Multivariate Variational Mode Decomposition

Kang Xing ^{1,2,3} , Shiyao Li ^{4,5}, Zhijie Qu ^{1,2,3} and Xiaojuan Zhang ^{1,2,*}

¹ Aerospace Information Research Institute, Chinese Academy of Sciences, Beijing 100094, China; xingkang19@mails.ucas.ac.cn (K.X.); quzhijie20@mails.ucas.ac.cn (Z.Q.)

² Key Laboratory of Electromagnetic Radiation and Sensing Technology, Chinese Academy of Sciences, Beijing 100190, China

³ School of Electronic, Electrical and Communication Engineering, University of Chinese Academy of Sciences, Beijing 100049, China

⁴ Tianjin Navigation Instruments Research Institute, Tianjin 300131, China; lishiyao18@mails.ucas.ac.cn

⁵ Tianjin Key Laboratory of Special Severe Environment Computer, Tianjin 300131, China

* Correspondence: xjzhang@aircas.ac.cn; Tel.: +86-10-5888-7276

Abstract: Noise suppression is essential in time-domain electromagnetic (TDEM) data processing and interpretation. TDEM data are typically in broadband signal, which makes it difficult to separate the signal in the whole frequency band. The conventional methods tend to process data trace by trace, ignoring the lateral continuity between channels. This paper proposes a workflow based on multivariate variational mode decomposition (MVMD) and multivariate detrended fluctuation analysis (MDFA) to deal with the noise in 2-D TDEM data. The proposed method initially employs MVMD to decompose TDEM signals into a series of intrinsic mode functions (IMFs). Subsequently, MDFA is used to calculate the scaling exponent of each IMF, facilitating the selection of signal-dominant IMFs. Finally, the signal IMFs are summed up to reconstruct the TDEM signal. Both simulation and field results demonstrate that, by considering the lateral continuity of data across channels, the proposed method is more effective at noise removal than other single-channel data processing techniques.

Keywords: time-domain electromagnetic; subsurface target detection; multivariate variational mode decomposition (MVMD); denoising



Citation: Xing, K.; Li, S.; Qu, Z.;

Zhang, X. Time-Domain

Electromagnetic Noise Suppression

Using Multivariate Variational Mode

Decomposition. *Remote Sens.* **2024**, *16*,

806. [https://doi.org/10.3390/](https://doi.org/10.3390/rs16050806)

rs16050806

Academic Editor: Roberto Orosei

Received: 19 January 2024

Revised: 23 February 2024

Accepted: 23 February 2024

Published: 25 February 2024



Copyright: © 2024 by the authors.

Licensee MDPI, Basel, Switzerland.

This article is an open access article

distributed under the terms and

conditions of the Creative Commons

Attribution (CC BY) license ([https://creativecommons.org/licenses/by/](https://creativecommons.org/licenses/by/4.0/)

[https://creativecommons.org/licenses/by/](https://creativecommons.org/licenses/by/4.0/)

4.0/).

1. Introduction

In recent years, the time-domain electromagnetic (TDEM) method has seen a surge in popularity across various fields, including geological research [1–3], environmental investigation [4–6], and unexploded ordnance detection [7–9], due to its non-destructive nature, cost-effectiveness, and ease of use. However, the noise in TDEM data significantly reduces the signal-to-noise ratio (SNR), impacting data quality and complicating processing and interpretation. TDEM signals exhibit a broad frequency band and non-linearity and non-stationarity characteristics, particularly becoming weak and susceptible to noise interference in the late stage.

Currently, two predominant methods exist for noise reduction in TDEM data, with the first being machine learning-based noise reduction. Methods for reducing noise in machine learning include utilizing sparse dictionary distributions [10,11] and various deep learning techniques [12–14]. Deep learning methods are particularly advantageous since they can automatically learn features from data, avoiding reliance on subjective human-selected data. They have gradually emerged as the mainstay of modern machine learning methods. Asif et al. developed an expert system based on a deep convolutional auto-encoder to eliminate interference from power lines, fences, and other structures in data [15]. Pan et al. proposed an encoder architecture that combines one-dimensional convolution

and vision transformers, retaining both the local perceptual features of convolutional networks and the global perceptual features of transformers. This architecture integrates a multi-task loss function and a densely connected residual structure to optimize noise reduction performance [16]. Chen et al. [17] proposed a deep convolutional neural network CNN-based denoiser to model the noise estimation image for different signal features. Wang et al. [18] suggested employing generative adversarial networks to construct a dataset and train a deep neural network-based denoiser to learn the mapping from noisy TDEM signals to the corresponding noise-free signals. Yu et al. [19] proposed the CG-DAE, a CNN-GRU Dual Auto-Encoder designed for 2-D TDEM data processing. This model processes 2-D TDEM response data as an image input network, improving data processing efficiency. Nevertheless, challenges arise from incorporating deep learning into TDEM data processing. These include high computational costs, the need for parameter adjustments, and performance variations depending on architecture and training data size.

The second method is based on signal decomposition, which offers more convenience and less computational intensity than machine learning-based approaches. Ji et al. initially employed a wavelet threshold to remove background noise from TDEM data, then identified and processed the details after the stationary wavelet transform (WT), and finally reconstructed the denoised TDEM data using an inverse stationary wavelet transform [20]. Wang et al. used empirical mode decomposition (EMD) to decompose TDEM signals under strong noise into multiple intrinsic mode functions (IMFs). They successfully extracted weak signals by employing power detection to extract and reduce the principal components of the noise, thereby enhancing the depth and accuracy of TDEM detection [21]. Liu et al. used ensemble empirical mode decomposition (EEMD) to suppress the motion noise of aviation transient electromagnetic [22]. Feng et al. first utilized the whale optimization algorithm (WOA) to obtain the optimal combination of modal decomposition number K and penalty factor α . Subsequently, they applied variational mode decomposition (VMD) for signal decomposition and finally used the Bhattacharyya distance algorithm to distinguish between effective and noise modes, accurately reconstructing the signal [23].

However, these methods have certain limitations. The WT method needs to select the appropriate wavelet basis function according to the characteristics of signal, which lacks self-adaptability and loses signal information in the decomposition process [24–26]. Although the EMD method and its variations do not require a priori information, they tend to cause modal aliasing and the decomposed IMFs are easily contaminated by noise. VMD can estimate multiple modes simultaneously in a non-recursive way, which ensures the completeness of the characteristics and improves the computational efficiency [27]. Using VMD and its improved method to decompose TDEM data can filter out noise and reconstruct signal accurately [28]. Nevertheless, a TDEM signal usually is a multi-channel signal, and the existing methods process TDEM data trace by trace, ignoring the continuity of data between channels.

Multivariate variational mode decomposition (MVMD) is a method for decomposing multichannel data [29]. MVMD processes TDEM data across multiple channels in unison, extracting IMFs that share identical center frequencies and bandwidths across various channels [30]. This concurrent processing of multichannel TDEM data enhances IMF continuity and aids in extracting spatial data features, effectively reducing noise [31]. This paper proposes a multichannel workflow for denoising TDEM data using MVMD and multivariate detrended fluctuation analysis (MDFA). Initially, we utilized MVMD to decompose 2-D TDEM signals into a series of IMFs. We then applied MDFA to calculate the scaling exponent of each group of IMFs, using these indices to select signal-dominant IMFs. The final step involved summing the selected signal IMFs to reconstruct the signal. We generated 2-D TDEM data and introduced varying levels of noise. The processing results indicate that the proposed method effectively removes noise, achieving a higher SNR by considering the lateral continuity between channels. The proposed method more accurately restores anomalous shapes compared to methods that process data channel by channel.

The processing of field data further confirms that the method effectively eliminates noise in early- and late-stage TDEM data.

2. Methods

In this section, we first briefly introduce the related mathematical theories and expressions. Then, we propose an MVMD-based MDFA workflow to separate and attenuate the random noise contained in the raw TDEM data. Next, we introduce the method for selecting parameters of MVMD. Finally, we provide further elucidation of the workflow, as shown in Algorithm 1.

Algorithm 1 TDEM signal denoising with MVMD-MDFA

Require: 2-D TDEM signal $\mathbf{x}(t)$

Ensure: Denoised 2-D TDEM signal $\mathbf{x}_{denoise}(t)$

- 1: set $K_{min}, K_{max}, \alpha = 2000, n = 0, \epsilon = 10^{-7}$
 - 2: **for** $k = K_{min}; k < K_{max}, k = k + 1$ **do**
 - 3: applying MVMD and calculating the correlation coefficients μ_k
 - 4: **if** $\mu_k \geq \text{threshold}$ **then**
 - 5: $K_{best} = k - 1$
 - 6: **end if**
 - 7: **end for**
 - 8: **while** $\sum_k \sum_c \frac{\|u_{k,c}^{n+1} - u_{k,c}^n\|_2^2}{\|u_{k,c}^n\|_2^2} < \epsilon$ **do**
 - 9: $n = n + 1$
 - 10: **for** $k = 1; k < K_{best}, k = k + 1$ **do**
 - 11: **for** $c = 1; c < C, c = c + 1$ **do**
 - 12: $u_{k,c}^{n+1} = \arg \min_{u_{k,c}} \mathcal{L}(\{u_{i < k, c}^{n+1}\}, \{u_{i \geq k, c}^n\}, \{\omega_i^n\}, \lambda_c^n)$
 - 13: **end for**
 - 14: **end for**
 - 15: **for** $k = 1; k < K_{best}, k = k + 1$ **do**
 - 16: $\omega_k^{n+1} = \arg \min_{\omega_k} \mathcal{L}(\{u_{i, c}^{n+1}\}, \{\omega_{i < k}^{n+1}\}, \{\omega_{i \geq k}^n\}, \lambda_c^n)$
 - 17: **end for**
 - 18: **for** $c = 1; c < C, c = c + 1$ **do**
 - 19: $\lambda_c^{n+1} = \lambda_c^n + \tau(x_c - \sum_k u_{k,c}^{n+1})$
 - 20: **end for**
 - 21: **end while**
 - 22: **for** $k = 1; k < K_{best}, k = k + 1$ **do**
 - 23: calculating the scaling exponent β_k of IMF_k
 - 24: **end for**
 - 25: calculating the slope of β , summing the IMFs preceding the point of maximum slope.
-

2.1. Multichannel Variational Mode Decomposition

The multivariate variational mode decomposition is an extension of the VMD method designed for multichannel data processing [32]. By simultaneously processing multichannel TDEM data, the MVMD algorithm enables the effective extraction of spatial features while enhancing the lateral continuity of data across channels. The principle of MVMD is as follows.

MVMD decomposes the 2-D TME signal $\mathbf{d}(t) = [d_1(t), d_2(t), \dots, d_C(t)]$ into K IMFs $\mathbf{u}_k(t)$.

$$\mathbf{d}(t) = \sum_{k=1}^K \mathbf{u}_k(t), \quad (1)$$

where $\mathbf{d}(t)$ contains C channels, each containing N sampling points.

And the k -th $\mathbf{u}_k(t)$ can be represented as

$$\mathbf{u}_k(t) = \begin{bmatrix} u_{k,1}(t) \\ u_{k,2}(t) \\ \vdots \\ u_{k,C}(t) \end{bmatrix} = \begin{bmatrix} f_{k,1}(t)e^{j\phi_{k,1}(t)} \\ f_{k,2}(t)e^{j\phi_{k,2}(t)} \\ \vdots \\ f_{k,C}(t)e^{j\phi_{k,C}(t)} \end{bmatrix}, \quad (2)$$

where $f_{k,C}(t)$ and $\phi_{k,C}(t)$ denote amplitude function and phase function corresponding to the C -th channel of $\mathbf{u}_k(t)$.

The aim of MVMD is to extract a collection of multivariate modulated modes $\mathbf{u}_k(t)|_{k=1}^K$ with two key criteria: (i) minimizing total bandwidths of modes extracted from input data, and (ii) ensuring that the sum of derived oscillations accurately reconstructs the original signal $\mathbf{u}_k(t)$.

The constrained optimization strategy can be expressed as

$$\begin{aligned} \min_{u_{k,c}, \omega_k} & \left\{ \sum_{k=1}^K \sum_{c=1}^C \left\| \partial_t [u_{k,c}(t) + \mathcal{H}u_{k,c}(t)] e^{-j\omega_k t} \right\|_2^2 \right\}, \\ \text{s.t.} & \sum_{k=1}^K u_{k,c}(t) = d_c(t), \quad c = 1, 2, \dots, C \end{aligned} \quad (3)$$

where $u_{k,c}(t)$ and $\mathcal{H}u_{k,c}(t)$ denote the k -th IMF of the c -th channel signal $d_c(t)$ and its Hilbert transform; ∂_t represents the partial derivative of time; ω_k denotes the central frequency of $u_{k,c}(t)$.

Then, an augmented Lagrangian is formulated to solve the optimization problem expressed as (3). This is achieved by adding two penalty terms to the Lagrangian: a quadratic term that enforces accuracy in reconstruction, and a Lagrangian multiplier λ term that ensures strict compliance with constraints.

$$\begin{aligned} \mathcal{L}(\{u_{k,c}\}, \{\omega_k\}, \{\lambda_c\}) & \\ = \alpha & \sum_{k=1}^K \sum_{c=1}^C \left\| \partial_t [u_{k,c}(t) + \mathcal{H}u_{k,c}(t)] e^{-j\omega_k t} \right\|_2^2 \\ & + \sum_{c=1}^C \left\| d_c(t) - \sum_{k=1}^K u_{k,c}(t) \right\|_2^2 + \sum_{c=1}^C \left\langle \lambda_c(t), d_c(t) - \sum_{k=1}^K u_{k,c}(t) \right\rangle, \end{aligned} \quad (4)$$

where $\langle a, b \rangle$ represents the inner product of a and b , λ_c represents the c -th channel of λ . The optimization problem is solved using the alternating direction method of multipliers (ADMMs), and the formula for updating $u_{k,c}$, $\omega_{k,c}$ and λ_c is given by:

$$\hat{u}_{k,c}^{n+1}(\omega) = \frac{\hat{d}_c(\omega) - \sum_{i \neq k} \hat{u}_{i,c}(\omega) + \frac{\hat{\lambda}_c(\omega)}{2}}{1 + 2\alpha(\omega - \omega_k)^2}, \quad (5)$$

$$\omega_k^{n+1} = \frac{\sum_{c=1}^C \int_0^\infty \omega |\hat{u}_{k,c}(\omega)|^2 d\omega}{\sum_{c=1}^C \int_0^\infty |\hat{u}_{k,c}(\omega)|^2 d\omega}, \quad (6)$$

$$\hat{\lambda}_c^{n+1}(\omega) = \hat{\lambda}_c^n(\omega) + \tau \left(\hat{d}_c(\omega) - \sum_{k=1}^K \hat{u}_{k,c}^{n+1}(\omega) \right), \quad (7)$$

where $\hat{u}_{k,c}$, \hat{d}_c and $\hat{\lambda}_c$ are the Fourier transform of $u_{k,c}$, d_c and λ_c . τ represents the parameter of noise tolerance. Update the above equation until it satisfies the following iteration termination condition:

$$\sum_{k=1}^K \sum_{c=1}^C \frac{\|\hat{u}_{k,c}^{n+1} - \hat{u}_{k,c}^n\|_2^2}{\|\hat{u}_{k,c}^n\|_2^2} < \epsilon, \quad (8)$$

where ϵ is the tolerance parameter of the convergence criterion.

2.2. Multichannel Detrended Fluctuation Analysis

TDEM signals, when decomposed via MVMD, produce a series of IMFs, requiring the introduction of auxiliary discriminant methods to select signal IMFs. Detrended fluctuation analysis (DFA) is extensively employed to identify scaling properties and detect long-range correlations in non-stationary time series, owing to its proficiency in detrending time series data [33]. MDFA simultaneously processes multichannel signals, enhancing the lateral continuity of data across channels [34]. Specifically, MDFA processes multichannel IMFs, effectively removing noise and trend components of various orders attributed to external factors.

For a given C -channel, time series $\mathbf{x}_i = [x_{i_1}, x_{i_2}, \dots, x_{i_C}]^T$ observation at time i , y_i is computed by

$$\mathbf{y}_i = \frac{1}{N} \sum_{i=1}^N (\mathbf{x}_i - \bar{\mathbf{x}}), \quad (9)$$

where $i = 1, 2, \dots, N$ donates the length of observation time, $\bar{\mathbf{x}} = \frac{1}{N} \sum_{i=1}^N \mathbf{x}_i$.

Next, $\mathbf{y}_i = y_{i_c} |_{c=1}^C$ for all observation time is divided in $2N_s$ disjoint intervals by cutting \mathbf{y}_i into $N_s = N/s$ segments sequentially and inversely. Then, the local trend $\tilde{\mathbf{y}}_i = y_{i_c} |_{c=1}^C$ is estimated based on the fitting polynomial of each channel

$$\tilde{y}_{i_c} = a_c \cdot i^2 + b_c \cdot i + c_c, \quad i = 1, \dots, s \quad (10)$$

where a_c, b_c, c_c are the coefficients of the quadratic term.

Then multivariate fluctuation $F_m^\Sigma(s)$ is formulated using Mahalanobis norm $\|\mathbf{y}_i - \tilde{\mathbf{y}}_i\|_\Sigma$

$$F_m^\Sigma(s) = \sqrt{\frac{1}{2sN_s} \sum_{v=1}^{2N_s} \sum_{i=vs+1}^{(v+1)s} (\mathbf{y}_i - \tilde{\mathbf{y}}_i)^T \Sigma^{-1} (\mathbf{y}_i - \tilde{\mathbf{y}}_i)}, \quad (11)$$

where covariance matrix Σ delineates the interchannel dependencies within the detrend $\mathbf{y}_i - \tilde{\mathbf{y}}_i$.

If the time series is long-range-correlated, it would be reflected in the function $F_m^\Sigma(s)$

$$F_m^\Sigma(s) = s^\beta, \quad (12)$$

Finally, scaling exponent β is calculated by the slope of $\ln F_m^\Sigma(s)$ and $\ln s$. The signal IMFs and noise IMFs can be screened out by the slope of β , then summing the signal IMFs to reconstruct the signal.

2.3. Parameter Selection

This section elaborates on the selection of pivotal parameters for MVMD. The number of modes to be decomposed, denoted as K , is crucial for MVMD's efficacy. To circumvent issues of over or under-decomposition, K is determined based on a dual criterion: a low correlation coefficient and minimal energy loss. Specifically, the correlation coefficient threshold is set at 0.4, and the number of modes for decomposition is chosen within the range from K_{min} to K_{max} . MVMD is applied iteratively within this defined range. If the correlation coefficient between the decomposed IMFs exceeds this threshold, it indicates over-decomposition. The optimal decomposition mode, K_{best} , is then considered one less than the current K . Furthermore, the bandwidth of the extracted modes is governed by the parameter α ; a smaller α results in a broader bandwidth. We set α to 2000 to improve

the fidelity of the constructed IMFs. Lastly, ϵ signifies the tolerance error between the raw TDEM data and the decomposed IMFs, and we set ϵ at 10^{-7} .

3. Synthetic Results

Synthetic TDEM data were generated to evaluate the effectiveness of the proposed workflow, as depicted in Figure 1a. The survey area is 5 m wide from east to west and 10 m long from north to south. The east–west profile comprises 20 channels, each encompassing 200 measurement points along the north–south direction. To simulate pipes of different diameters and different burial depths, responses from large, medium, and small-sized pipelines were created at distances of 8, 5, and 2 m to the north, respectively. Then, 0 dB Gaussian white noise was added to the synthetic TDEM data. Notably, the responses at 8 m and 2 m can be observed, but the anomaly shapes are not clear, and the response at 5 m is minimally visible, as shown in Figure 1b.

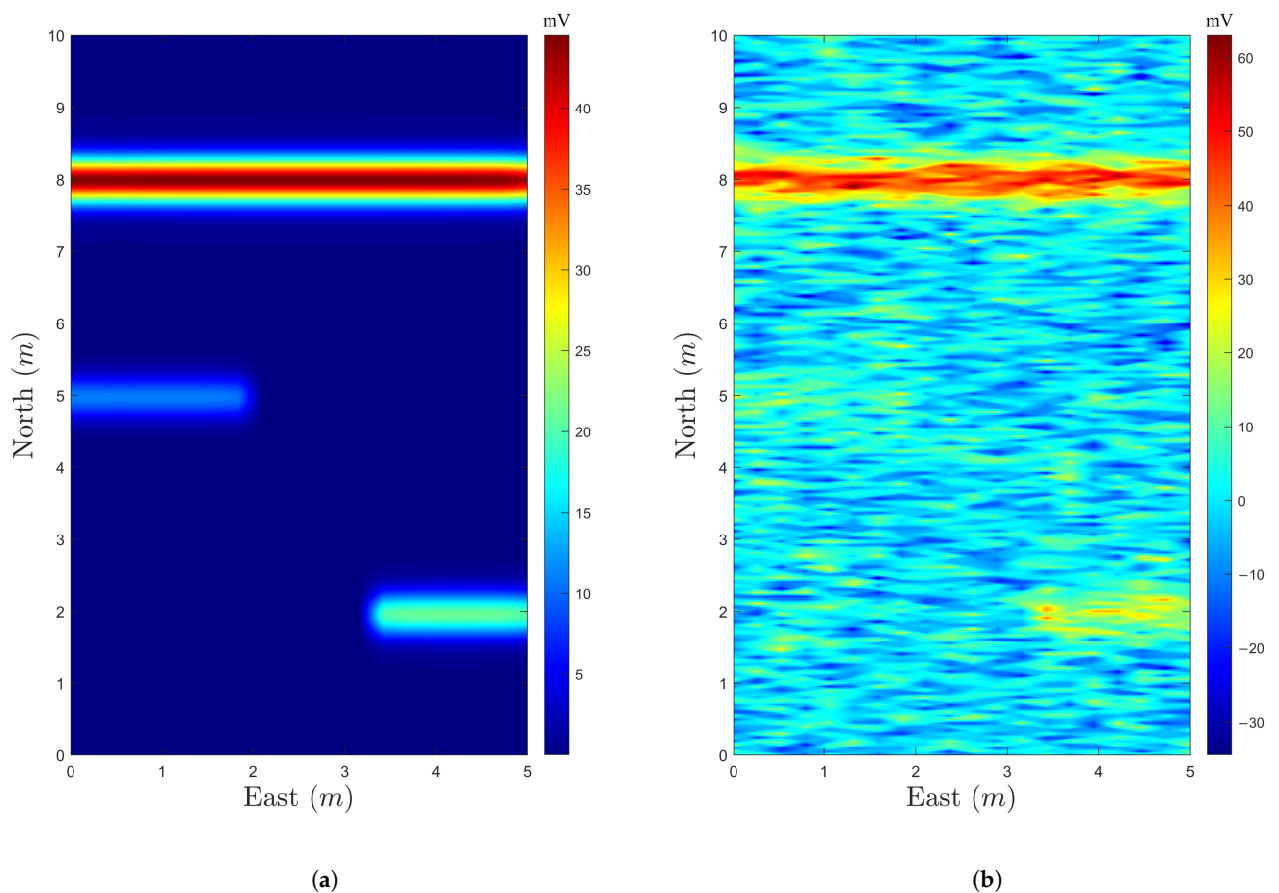


Figure 1. Synthetic 2-D TDEM data. (a) Noise-free data. (b) Data with 0 dB random noise.

Next, we applied MVMD to the noisy data and extracted a series of IMFs, as illustrated in Figure 2. These IMFs are sequentially organized from low to high frequency. Analysis of the graph reveals that the low-frequency IMFs encompass more energy, signifying the underlying trend of change, while the high-frequency IMFs, although noisier, provide finer details. As evidenced in Figure 2a, at the exact locations of the simulated pipeline responses in the original data, corresponding anomalies are discernible in IMF1, ensuring continuity across adjacent channels. In IMF1, the 160th point across all channels exhibits the maximum response, corresponding to the response of the pipeline that traverses all channels at 8 m in the original data; the responses at points 40 and 100 have similar characteristics. This observation is consistent in IMF2. However, due to increased frequency in IMFs 3 to 9, the anomalous responses indicative of the pipelines become indistinct.

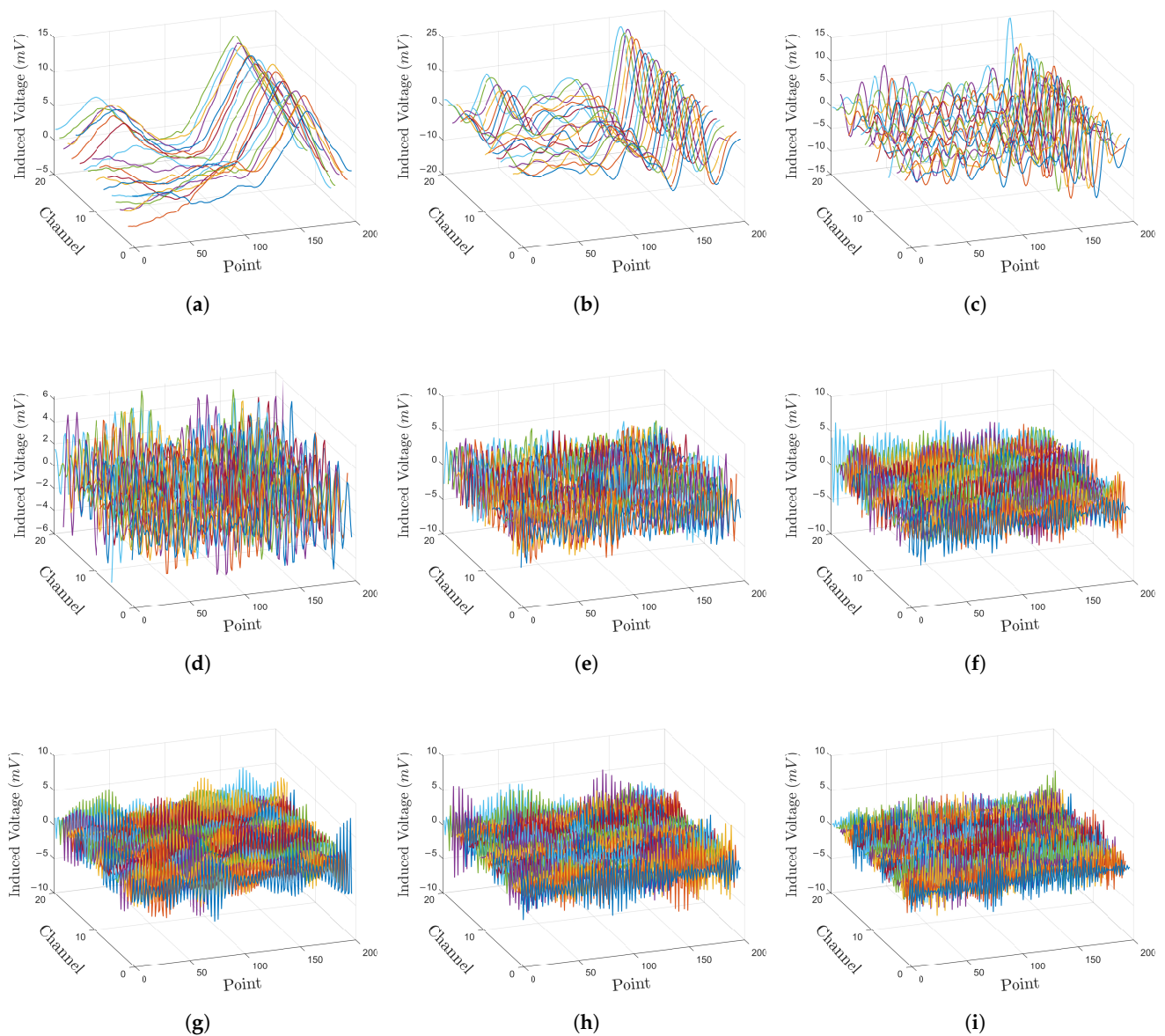


Figure 2. IMFs decomposed from synthetic TDEM data by MVMD. (a–i) IMF1–IMF9.

Subsequently, MDFA is conducted on all IMFs to calculate the scaling exponent, β , which serves as a criterion to differentiate between signal-dominated and noise-dominated IMFs. The slope of β signifies the reduction in long-range correlation, with a higher slope indicating a substantial increase in noise content. Consequently, IMFs preceding the point of maximum slope are deemed to predominantly contain relevant signals. In Figure 3, the red line marks the maximum slope point, identifying IMF1 to IMF4 as signal-dominated.

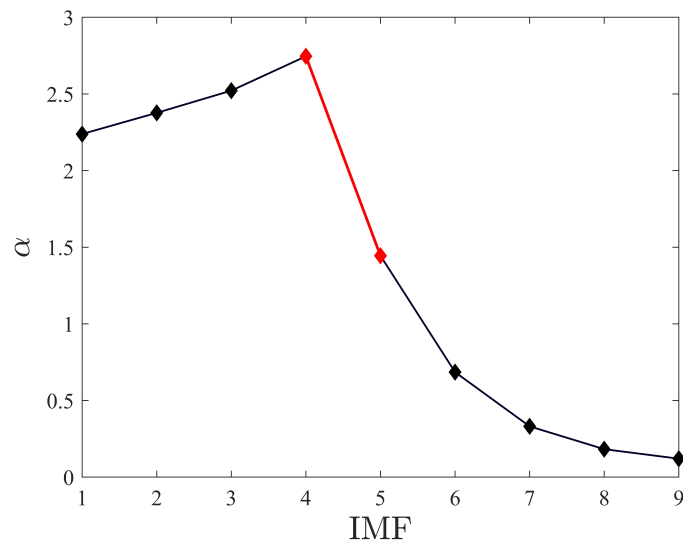


Figure 3. Scaling exponent of various IMFs decomposed from synthetic TDEM data.

Finally, the signal-dominated IMFs are summed to obtain the TDEM signal after removing the noise. We showcase the signal processing details before and after for channels 2 and 14 and compare these with the results from other methods. As observed in Figure 4, although the responses from the large and medium pipelines are significant, they are still severely interfered with by noise, and the response of the small pipeline is submerged in noise. The proposed method effectively removes the noise, restoring the responses of the large and medium pipelines and accurately extracting the response of the small pipeline.

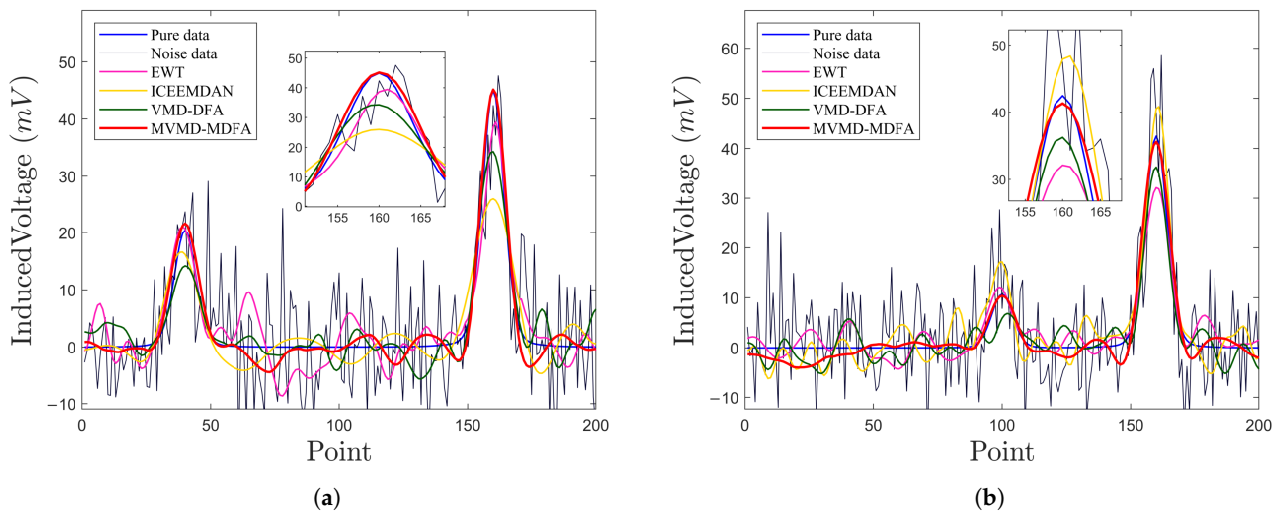


Figure 4. Synthetic TDEM denoised results of different methods for channel 2 (a) and channel 14 (b).

Subsequently, we visualized the denoised data and compared it with the results obtained from other methods. As shown in Figure 5, anomalies can be identified in all four images, each exhibiting distinct morphologies. The proposed method eliminates noise, resulting in a noticeably cleaner image. More importantly, it accurately extracts weak responses previously obscured by noise while maintaining the continuity of anomalous shapes across channels. In contrast, the results processed by other methods exhibit discontinuities in the anomalous forms, failing to reconstruct the characteristics of the pipelines accurately.

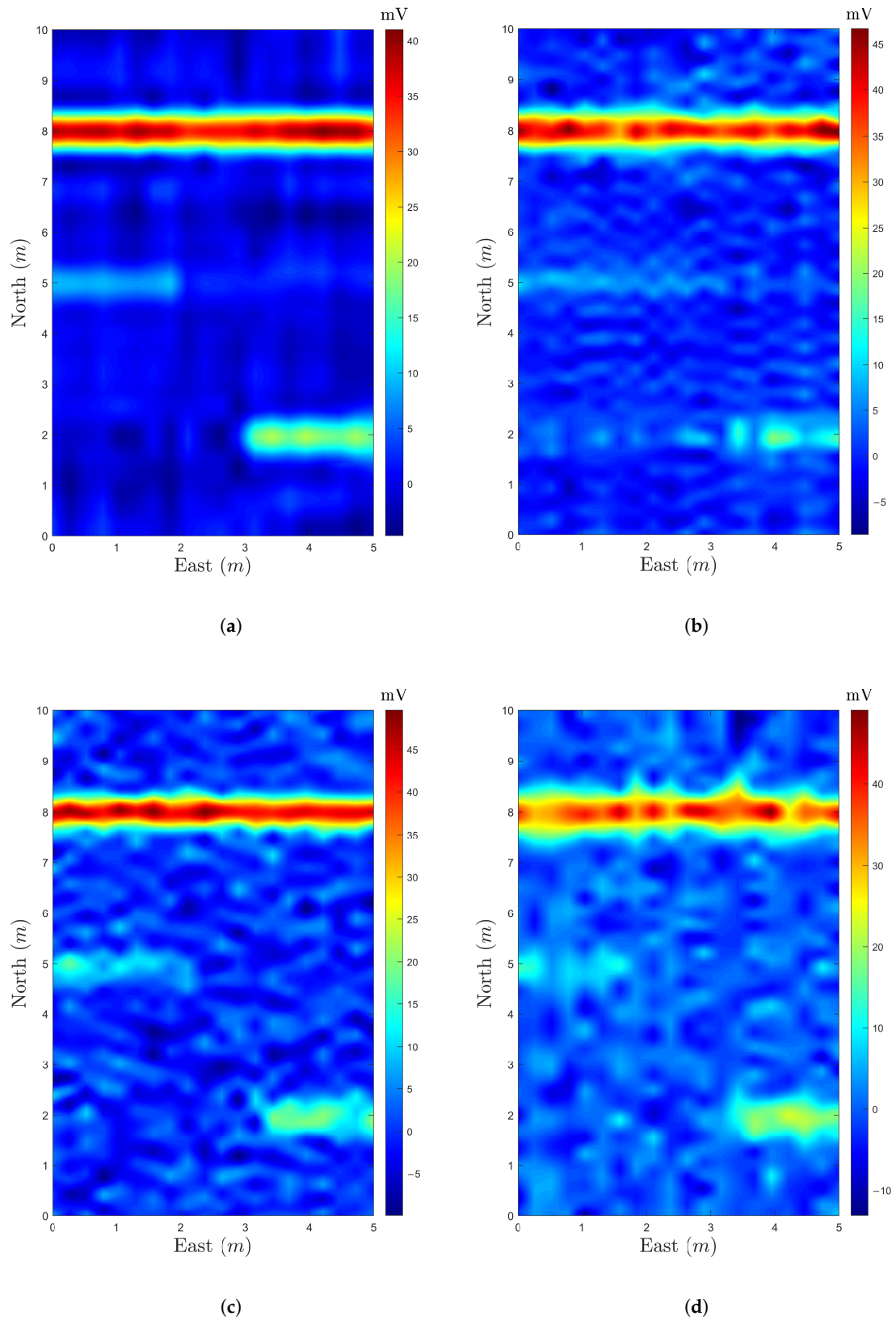


Figure 5. Synthetic TDEM denoised results of different methods for all channels. (a) MVMD-MDFA; (b) VMD-DFA; (c) EWT; (d) ICEEMDAN.

We also processed the data containing 5 dB and 10 dB noise levels using various methods, with the results displayed in Table 1. The outcomes obtained with the proposed method surpassed those of other methods across different noise levels, thereby validating its effectiveness. The time costs by different methods are shown in Table 2, where the proposed method takes the longest time. Compared to other single-channel methods, the proposed method considers all channels as a set and the inter-channel correlations, increasing the time required for iteration.

Table 1. SNR of synthetic data processed by different methods.

Methods	ICEEMDAN	EWT	VMD-DFA	Proposed Workflow
0 dB Noise	0.57	1.44	1.02	2.24
5 dB Noise	3.96	6.11	4.55	6.78
10 dB Noise	7.39	10.47	9.26	11.12

Table 2. Time costs of synthetic data processed by different methods.

Methods	ICEEMDAN	EWT	VMD-DFA	Proposed Workflow
Time costs (s)	26.7	1.04	7.2	30.4

4. Experimental Results

4.1. System Description

The TDEM system, depicted in Figure 6, developed by the Aerospace Information Research Institute at the Chinese Academy of Sciences validated the algorithm. This system consists of a transmitting module, a data acquisition module, and a positioning module. It features a square transmitting coil measuring 1 m on each side and three concentric square receiving coils, each with a side length of 0.5 m. The location of the sensor is precisely determined by a Real-Time Kinematic (RTK) module positioned at the center of the receiving coil, achieving a positioning accuracy of less than 1 cm.

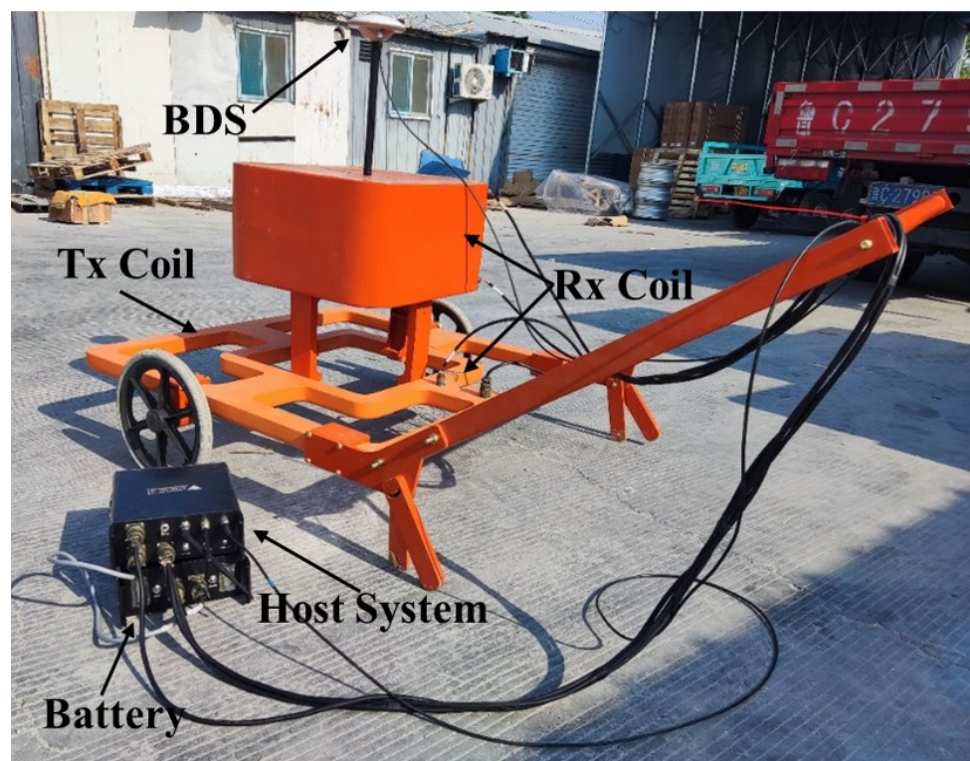


Figure 6. The TDEM detection system used to verify the proposed method.

4.2. Test Field Result

Verification experiments were conducted in Liaocheng, Shandong, China. Approximately 1 m beneath the experimental site, a steel gas pipeline with a diameter of about 30 cm was buried. Four parallel measurement lines were planned, spaced approximately 1 m apart, as depicted by the red line in Figure 7. During these tests, the TDEM system moved at an approximate speed of 1 m per second.

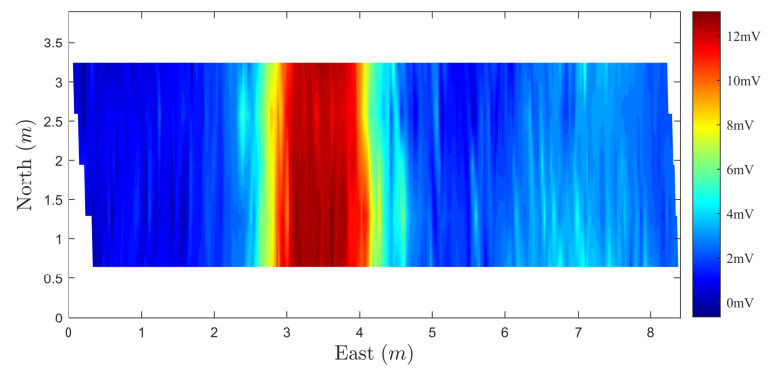


Figure 7. The experimental site with buried pipelines.

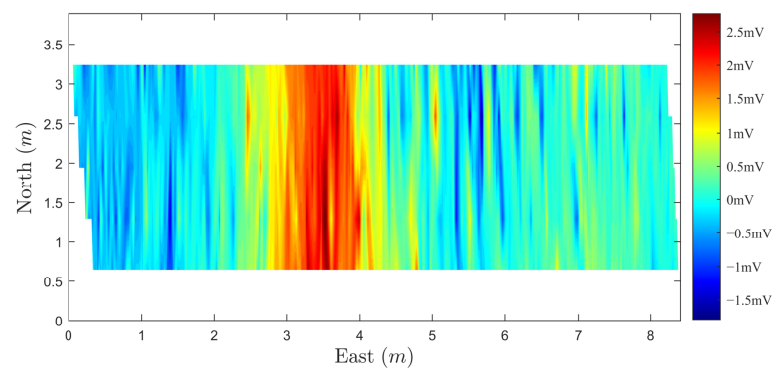
Upon completing the measurements, we rendered the original data in graphical form, as depicted in Figure 8. Figure 8a represents the early-stage data, which show that the anomalies have greater amplitude and are more distinct in shape due to a higher SNR in the early signals. However, noise interference results in some roughness at the edges. Figure 8b displays the late-stage data. Over time, the SNR in these stages decreases, and although anomalies remain visible, their precise shapes become indiscernible.

We established the optimal modal decomposition number as 6 and applied MVMD to both early- and late-stage data. This process yielded a series of IMFs, which are depicted in Figures 9 and 10, respectively. From Figure 8, it is evident that due to the differences in signal characteristics between early and late stages, the features of the IMFs obtained from decomposition also differ. In the early-stage signals, IMF1 and IMF2 have higher SNR with distinct anomaly shapes, whereas in the late-stage signals, only the anomaly shape of IMF1 is distinctive.

Subsequently, we employed MDFA to calculate the scaling indices of the IMFs for both early and late stages, with the results displayed in Figure 11. Based on the scaling indices, we reconstructed the early-stage signal by summing IMF1 to IMF3, and the late-stage signal by summing IMF1 and IMF2.

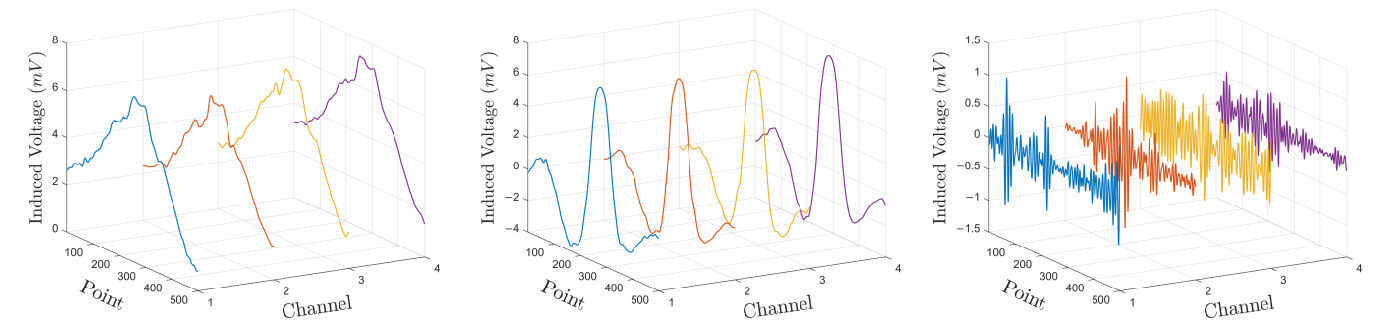


(a)



(b)

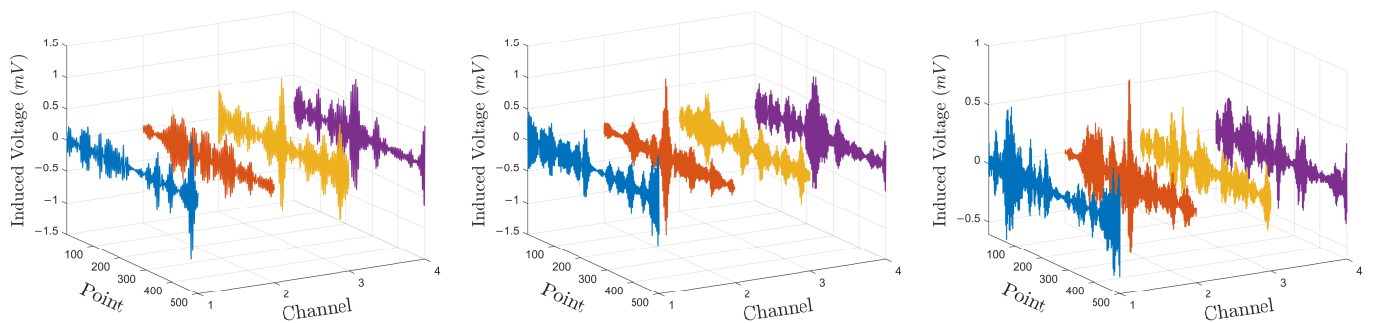
Figure 8. Early- and late-stage TDEM signals. (a) Early-stage. (b) Late-stage.



(a)

(b)

(c)



(d)

(e)

(f)

Figure 9. IMFs obtained from early-stage TDEM signal through MVMD. (a–f) IMF1–IMF6.

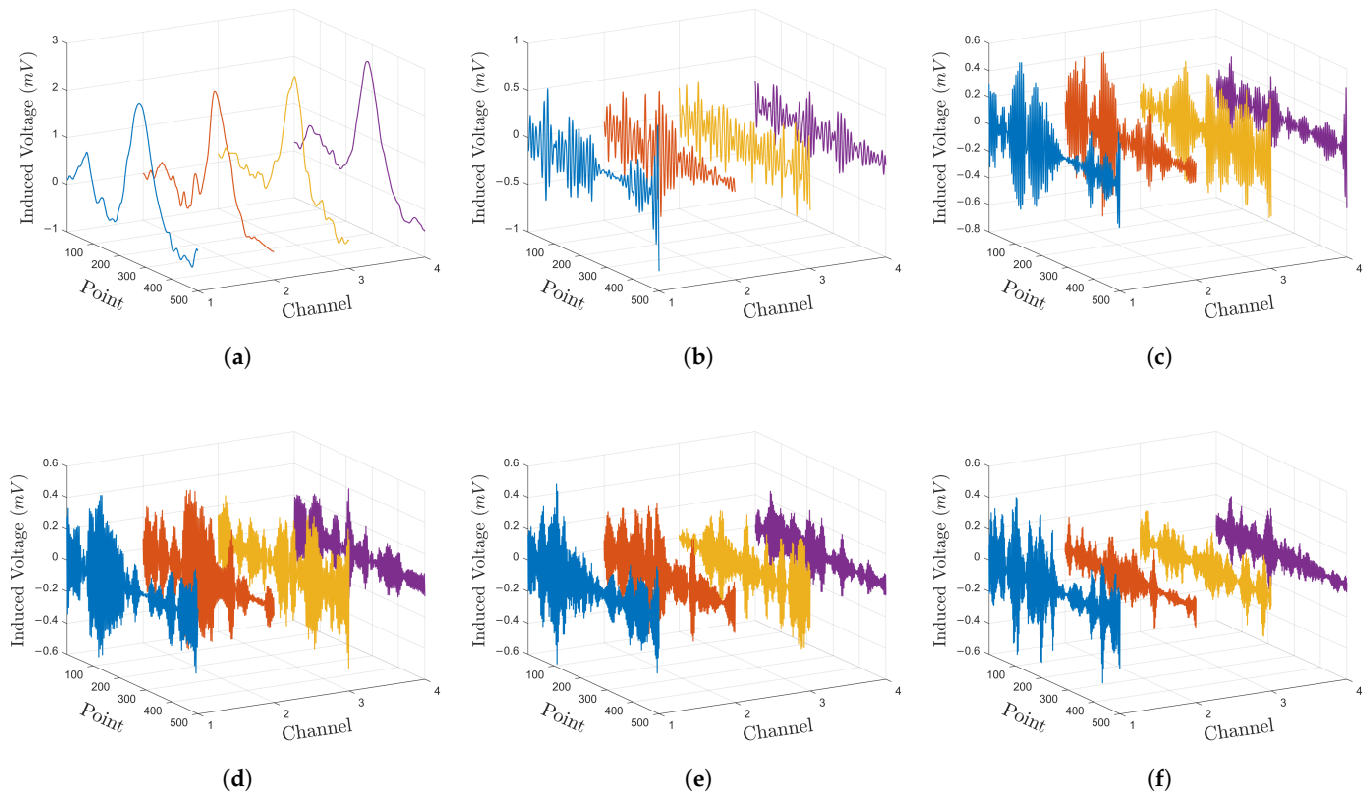


Figure 10. IMFs obtained from late-stage TDEM signal through MVMD. (a–f) IMF1–IMF6.

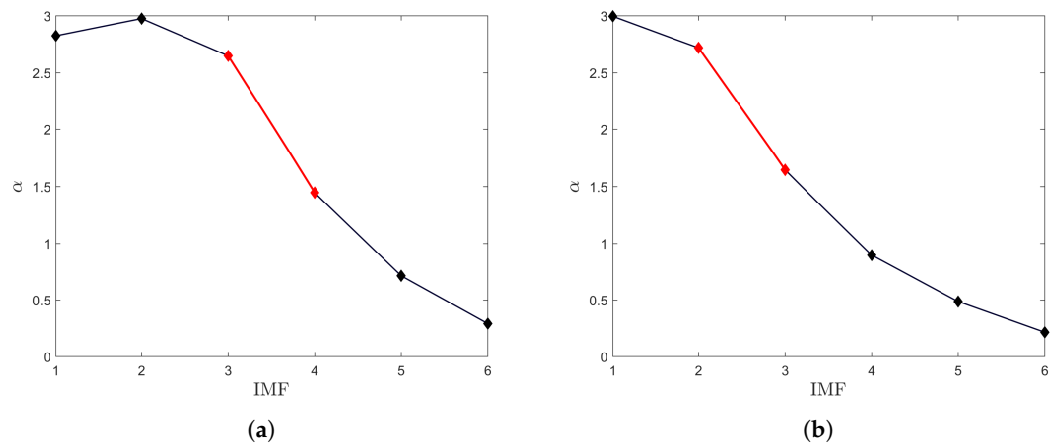


Figure 11. The scaling exponent of IMFs decomposed from early- and late-stage TDEM signals. (a) Early-stage. (b) Late-stage.

The denoised early- and late-stage signals are presented in Figure 12. It is observable that in the denoised early-stage signals, the pipeline response shape is complete, and the edges are more precise; in the late-stage signals, the SNR has dramatically improved, accurately extracting the pipeline response from the noise, demonstrating the effectiveness of the proposed workflow in eliminating noise and restoring the abnormal shape of the pipeline.

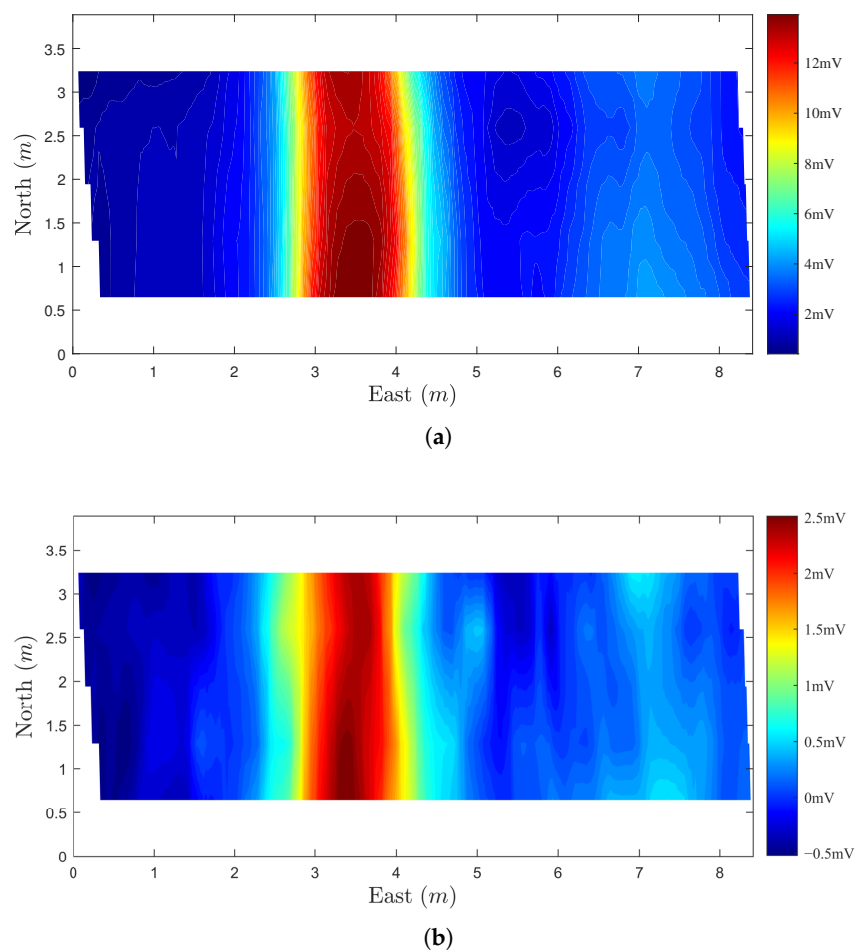


Figure 12. Denoised early- and late-stage TDEM signals. (a) Early-stage. (b) Late-stage.

5. Discussion

In TDEM survey tasks, when the scale of subsurface anomalies is substantially large relative to the detection equipment utilized, this scenario typically yields analogous anomalous responses across multiple survey lines, highlighting a prevalent issue in geophysical exploration. The inherent wide dynamic range of TDEM data further complicates the scenario as later-stage data become increasingly prone to a spectrum of interferences, including environmental noise, equipment-induced artifacts, and signal attenuation. Traditional approaches in signal processing predominantly focus on decomposing data trace by trace without addressing the lateral continuity of data between adjacent channels, potentially overlooking significant subsurface features.

This paper pioneers a multichannel TDEM data processing methodology combining MVMD and MDFA. Contrary to VMD and similar single-channel processing methods, which process data trace by trace, our method astutely extracts IMFs with uniform center frequencies across all channels. This critical advancement ensures the preservation and enhancement of lateral data continuity between channels. This approach addresses the challenges above by exploiting the spatial coherence inherent in geophysical datasets.

Simulation studies meticulously crafted identical pipeline responses in adjacent channels, mirroring real-world scenarios of significant subsurface anomalies. To emulate varying degrees of signal fidelity, we introduced three distinct amplitude levels—high, medium, and low—each representing different SNRs. This setup allowed us to rigorously evaluate the efficacy of our proposed method against conventional techniques. After undergoing MVMD processing, the simulated TDEM data yielded a series of IMFs, as shown in Figure 2, where IMF1 consistently exhibits analogous amplitudes and trends across

different channels, thereby reinforcing the spatial continuity of the subsurface anomaly signal. Subsequent application of MDFA enables the calculation of scaling indices for the various IMFs. By selecting signal IMFs before the maximum reduction in long-range correlations for summation, we effectively complete the signal denoising process, thereby significantly enhancing the signal clarity and interpretability of TDEM data. The efficacy of our proposed methodology is vividly demonstrated in Figure 5a, where continuous anomalous patterns emerge with remarkable clarity, successfully recovering data previously obscured by noise. The efficacy of this multichannel approach is further corroborated by Table 1, which showcases superior performance metrics across varying SNRs. Then, we used a TDEM system to measure the response of underground gas pipelines, and field data analysis reinforces the method's robustness, effectively mitigating noise in both early- and late-stage TDEM data, thus accurately depicting the morphology of subsurface targets.

During our evaluation, traditional VMD processing clocked in at 7.2 s, while our novel approach required 30.4 s. The MDFA took 1.6 s, and MVMD accounted for 28.8 s, because of its holistic treatment of all channel data as a unified entity and meticulous consideration of inter-channel correlations. This approach necessitates more iterations, extending the computation time required for the ADMM to converge on the optimization problem. The selection of the parameter α , pivotal for the decomposition's effectiveness, is manually determined based on the specific demands of the dataset, representing a potential area for optimization.

Our future work is poised to delve into more efficient optimization methodologies to reduce computational overhead. Furthermore, we are committed to developing refined criteria for selecting MVMD parameters. Additionally, we will explore other multichannel data processing methods, such as multivariate iterative filtering [35] and multichannel adaptive Fourier decomposition [36], which do not require prior information and exhibit higher robustness to enhance the effectiveness and utility of multichannel TDEM data processing techniques in geophysical exploration.

6. Conclusions

This paper introduces a noise reduction method for multichannel TDEM data. It involves decomposing 2-D TDEM data into a series of IMFs using MVMD, followed by MDFA to distinguish between signal and noise IMFs. The final denoising step is achieved by summing the selected IMFs. Multichannel TDEM data were generated, and various noise levels (0 dB, 5 dB, and 10 dB) were added to compare the effectiveness of different methods. The results indicate that the proposed method enhances lateral continuity between channels and accurately extracts anomalous signal features, effectively reducing noise. Using the TDEM system, we collected responses from underground pipelines. This process validated the proposed method's ability to effectively handle noise in both early- and late-stage data, significantly improving reliability and interpretability.

Author Contributions: Conceptualization, K.X. and X.Z.; methodology, K.X.; validation, K.X., S.L. and Z.Q.; formal analysis, X.Z.; investigation, K.X. and S.L.; resources, K.X., S.L. and Z.Q.; data curation, K.X.; writing—original draft preparation, K.X.; writing—review and editing, X.Z.; visualization, Z.Q.; supervision, X.Z.; project administration, X.Z.; funding acquisition, X.Z. All authors have read and agreed to the published version of the manuscript.

Funding: This research was funded by the National Natural Science Foundation of China, grant number 61172017.

Data Availability Statement: Data are contained within the article.

Conflicts of Interest: The authors declare no conflicts of interest.

Abbreviations

The following abbreviations are used in this manuscript:

TDEM	Time-domain electromagnetic
MVMD	Multivariate variational mode decomposition
MDFA	Multichannel detrended fluctuation analysis
IMF	Intrinsic mode function
SNR	Signal-to-noise ratio
WT	Wavelet transform
EMD	Empirical mode decomposition
EEMD	Ensemble empirical mode decomposition
WOA	Whale optimization algorithm
VMD	Variational mode decomposition
DFA	Detrended fluctuation analysis
EWT	Empirical wavelet transform
ICEEMDAN	Improved complete ensemble empirical mode decomposition with adaptive noise
RTK	Real-time kinematic

References

- Amato, F.; Pace, F.; Vergnano, A.; Comina, C. TDEM prospections for inland groundwater exploration in semiarid climate, Island of Fogo, Cape Verde. *J. Appl. Geophys.* **2021**, *184*, 104242. [[CrossRef](#)]
- Porras, D.; Carrasco, J.; Carrasco, P.; Herrero-Pacheco, J.L. Deep TDEM Study for Structural and Mining Purposes: A Case Study of the Barbastro Saline-Evaporitic Formation, Spain. *Appl. Sci.* **2023**, *13*, 6385. [[CrossRef](#)]
- Osinowo, O.O.; Fashola, O.E.; Ayolabi, E.A.; Olayinka, A.I. Structural mapping and gold mineralisation potential evaluation from airborne time-domain electromagnetic (TDEM) data of Ilesha Schist Belt, southwestern Nigeria. *Explor. Geophys.* **2022**, *53*, 237–254. [[CrossRef](#)]
- Baawain, M.S.; Al-Futaisi, A.M.; Ebrahimi, A.; Omidvarborna, H. Characterizing leachate contamination in a landfill site using Time Domain Electromagnetic (TDEM) imaging. *J. Appl. Geophys.* **2018**, *151*, 73–81. [[CrossRef](#)]
- Christensen, N.B.; Halkjær, M. Mapping pollution and coastal hydrogeology with helicopterborne transient electromagnetic measurements. *Explor. Geophys.* **2014**, *45*, 243–254. [[CrossRef](#)]
- Pellerin, L.; Beard, L.P.; Mandell, W. Mapping structures that control contaminant migration using helicopter transient electromagnetic data. *J. Environ. Eng. Geophys.* **2010**, *15*, 65–75. [[CrossRef](#)]
- Xie, W.; Zhang, X.; Mu, Y.; Zheng, Y. A subsurface targets' classification method utilizing gradient learning technique. *IEEE Geosci. Remote. Sens. Lett.* **2020**, *19*, 3000305. [[CrossRef](#)]
- Li, S.; Zhang, X.; Xing, K.; Zheng, Y. Fast inversion of subsurface target electromagnetic induction response with deep learning. *IEEE Geosci. Remote. Sens. Lett.* **2022**, *19*, 3006205. [[CrossRef](#)]
- Mu, Y.; Xie, W.; Zhang, X. The joint UAV-borne magnetic detection system and cart-mounted time domain electromagnetic system for UXO detection. *Remote Sens.* **2021**, *13*, 2343. [[CrossRef](#)]
- Li, G.; He, Z.; Tang, J.; Deng, J.; Liu, X.; Zhu, H. Dictionary learning and shift-invariant sparse coding denoising for controlled-source electromagnetic data combined with complementary ensemble empirical mode decomposition. *Geophysics* **2021**, *86*, E185–E198. [[CrossRef](#)]
- Li, G.; Wu, S.; Cai, H.; He, Z.; Liu, X.; Zhou, C.; Tang, J. IncepTCN: A new deep temporal convolutional network combined with dictionary learning for strong cultural noise elimination of controlled-source electromagnetic data. *Geophysics* **2023**, *88*, E107–E122. [[CrossRef](#)]
- Sun, Y.; Huang, S.; Zhang, Y.; Lin, J. Denoising of transient electromagnetic data based on the minimum noise fraction-deep neural network. *IEEE Geosci. Remote. Sens. Lett.* **2022**, *19*, 8028405. [[CrossRef](#)]
- Lin, F.; Chen, K.; Wang, X.; Cao, H.; Chen, D.; Chen, F. Denoising stacked autoencoders for transient electromagnetic signal denoising. *Nonlinear Process Geophys.* **2019**, *26*, 13–23. [[CrossRef](#)]
- Wu, X.; Xue, G.; He, Y.; Xue, J. Removal of multisource noise in airborne electromagnetic data based on deep learning. *Geophysics* **2020**, *85*, B207–B222. [[CrossRef](#)]
- Asif, M.R.; Maurya, P.K.; Foged, N.; Larsen, J.J.; Auken, E.; Christiansen, A.V. Automated Transient Electromagnetic Data Processing for Ground-Based and Airborne Systems by a Deep Learning Expert System. *IEEE Trans. Geosci. Remote Sens.* **2022**, *60*, 5919814. [[CrossRef](#)]
- Pan, D.; Qi, T.; Feng, G.; Wang, H.; Zhang, Z.; Wei, X. TEM1Dformer: A novel one-dimensional time series deep denoising network for TEM signals. *IEEE Sens. J.* **2024**, *24*, 414–426. [[CrossRef](#)]
- Chen, K.; Pu, X.; Ren, Y.; Qiu, H.; Lin, F.; Zhang, S. TEMDNet: A novel deep denoising network for transient electromagnetic signal with signal-to-image transformation. *IEEE Trans. Geosci. Remote Sens.* **2020**, *60*, 5900318. [[CrossRef](#)]
- Wang, M.; Lin, F.; Chen, K.; Luo, W.; Qiang, S. TEM-NLnet: A deep denoising network for transient electromagnetic signal with noise learning. *IEEE Trans. Geosci. Remote Sens.* **2022**, *60*, 5911714. [[CrossRef](#)]

19. Yu, S.; Shen, Y.; Zhang, Y. CG-DAE: A noise suppression method for two-dimensional transient electromagnetic data based on deep learning. *J. Geophys. Eng.* **2023**, *20*, 600–609. [[CrossRef](#)]
20. Ji, Y.; Li, D.; Yuan, G.; Lin, J.; Du, S.; Xie, L.; Wang, Y. Noise reduction of time domain electromagnetic data: Application of a combined wavelet denoising method. *Radio Sci.* **2016**, *51*, 680–689. [[CrossRef](#)]
21. Wang, G.F.; Deng, P.; Zhang, F.Q.; Ye, J.C. Noise reduction of the transient electromagnetic weak signal under strong noise based on power detection of EMD. *Appl. Mech. Mater.* **2012**, *110*, 1606–1612. [[CrossRef](#)]
22. Liu, F.; Li, J.; Liu, L.; Huang, L.; Fang, G. Application of the EEMD method for distinction and suppression of motion-induced noise in grounded electrical source airborne TEM system. *J. Appl. Geophys.* **2017**, *139*, 109–116. [[CrossRef](#)]
23. Feng, G.; Wei, H.; Qi, T.; Pei, X.; Wang, H. A transient electromagnetic signal denoising method based on an improved variational mode decomposition algorithm. *Measurement* **2021**, *184*, 109815. [[CrossRef](#)]
24. Wei, X.; Feng, G.; Qi, T.; Guo, J.; Li, Z.; Zhao, D.; Li, Z. Reduce the noise of transient electromagnetic signal based on the method of SMA-VMD-WTD. *IEEE Sens. J.* **2022**, *22*, 14959–14969. [[CrossRef](#)]
25. Qi, T.; Wei, X.; Feng, G.; Zhang, F.; Zhao, D.; Guo, J. A method for reducing transient electromagnetic noise: Combination of variational mode decomposition and wavelet denoising algorithm. *Measurement* **2022**, *198*, 111420. [[CrossRef](#)]
26. Lu, J.-Y.; Lin, H.; Ye, D.; Zhang, Y.-S. A new wavelet threshold function and denoising application. *Math. Probl. Eng.* **2016**, *2016*, 3195492.
27. Dragomiretskiy, K.; Zosso, D. Variational mode decomposition. *IEEE Trans. Signal Process.* **2013**, *62*, 531–544. [[CrossRef](#)]
28. Wei, H.; Qi, T.; Feng, G.; Jiang, H. Comparative research on noise reduction of transient electromagnetic signals based on empirical mode decomposition and variational mode decomposition. *Radio Sci.* **2021**, *56*, e2020RS007135. [[CrossRef](#)]
29. Ur Rehman, N.; Aftab, H. Multivariate variational mode decomposition. *IEEE Trans. Signal Process.* **2019**, *67*, 6039–6052. [[CrossRef](#)]
30. Liu, N.; Li, F.; Wang, D.; Gao, J.; Xu, Z. Ground-roll separation and attenuation using curvelet-based multichannel variational mode decomposition. *IEEE Trans. Geosci. Remote Sens.* **2021**, *60*, 5901214. [[CrossRef](#)]
31. Zhang, Y.; Zhang, H.; Yang, Y.; Liu, N.; Gao, J. Seismic Random Noise Separation and Attenuation Based on MVMD and MSSA. *IEEE Trans. Geosci. Remote Sens.* **2022**, *60*, 5908916. [[CrossRef](#)]
32. Li, G.; Zheng, H.; Cai, H.; Chen, C.; Shi, F.; Gong, S. Multi-channel geomagnetic signal processing based on deep residual network and MVMD. *Chin. J. Geophys.* **2023**, *66*, 3540–3556.
33. Mert, A.; Akan, A. Detrended fluctuation thresholding for empirical mode decomposition based denoising. *Digit. Signal. Process.* **2014**, *32*, 48–56. [[CrossRef](#)]
34. Naveed, K.; Mukhtar, S.; Rehman, N.U. Multivariate signal denoising based on generic multivariate detrended fluctuation analysis. In Proceedings of the 2021 IEEE Statistical Signal Processing Workshop (SSP), Virtual, 11–14 July 2021; pp. 441–445.
35. Cicone, A.; Pellegrino, E. Multivariate fast iterative filtering for the decomposition of nonstationary signals. *IEEE Trans. Signal Process.* **2022**, *70*, 1521–1531. [[CrossRef](#)]
36. Wang, Z.; Wong, C.M.; Rosa, A.; Qian, T.; Wan, F. Adaptive Fourier decomposition for multi-channel signal analysis. *IEEE Trans. Signal Process.* **2022**, *70*, 903–918. [[CrossRef](#)]

Disclaimer/Publisher’s Note: The statements, opinions and data contained in all publications are solely those of the individual author(s) and contributor(s) and not of MDPI and/or the editor(s). MDPI and/or the editor(s) disclaim responsibility for any injury to people or property resulting from any ideas, methods, instructions or products referred to in the content.